Article
http://justc.ustc.edu.cn Received: February 28, 2022; Accepted: April 02, 2022

Exploring the topological effect of linear and cyclic macroCTAs during polymerization-induced self-assembly (PISA)

Depeng Yin, Wen Xu, Hualong Zhang, Chao Liu ✉, and Chunyan Hong ✉

CAS Key Laboratory of Soft Matter Chemistry, Department of Polymer Science and Engineering, University of Science and Technology of China, Hefei 230026, China

✉Correspondence: Chao Liu, E-mail: liuchao216@ustc.edu.cn; Chunyan Hong, E-mail: hongcy@ustc.edu.cn

Graphical abstract

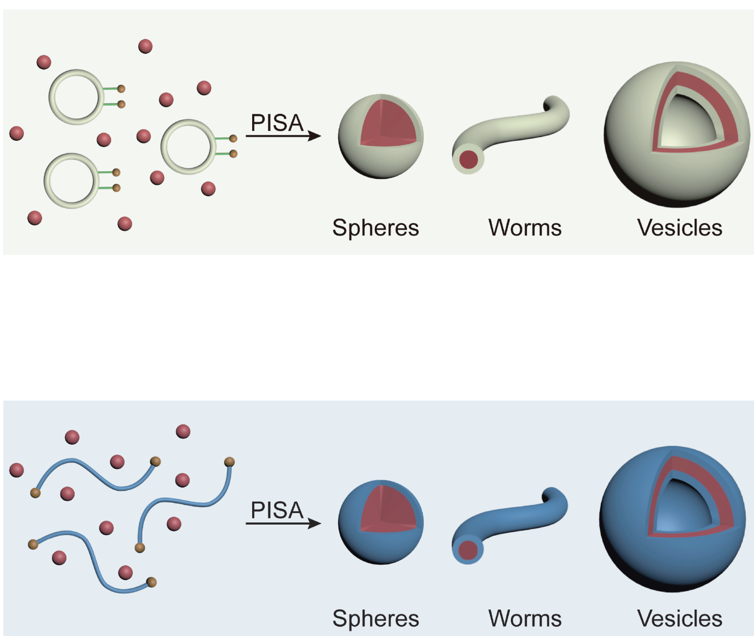

The cyclic hydrophilic segment can delay the morphological transition of block copolymer nanoparticles during PISA compared with the linear analog.

Public summary

- A cyclic macromolecular chain transfer agent (macroCTA) was synthesized via UV-induced cyclization.
- The effects of the topological structures of macroCTA on the polymerization kinetics and morphologies of block copolymer assemblies during reversible addition fragmentation chain transfer (RAFT) dispersion polymerization were explored.
- The cyclic hydrophilic segment could lead to a longer nucleation period and delay the morphology transition of block copolymer nanoparticles during PISA.

Citation: Yin D P, Xu W, Zhang H L, et al. Exploring the topological effect of linear and cyclic macroCTAs during polymerization-induced self-assembly (PISA). *JUSTC*, **2022**, 52(5): 1. DOI: 10.52396/JUSTC-2022-0040

JUSTC

Article

http://justc.ustc.edu.cn

Received: February 28, 2022; Accepted: April 02, 2022

Exploring the topological effect of linear and cyclic macroCTAs during polymerization-induced self-assembly (PISA)

Depeng Yin, Wen Xu, Hualong Zhang, Chao Liu ✉, and Chunyan Hong ✉

CAS Key Laboratory of Soft Matter Chemistry, Department of Polymer Science and Engineering, University of Science and Technology of China, Hefei 230026, China

✉Correspondence: Chao Liu, E-mail: liuchao216@ustc.edu.cn; Chunyan Hong, E-mail: hongcy@ustc.edu.cn

Cite This: *JUSTC*, **2022**, 52(5): 1 (9pp)

Read Online

Abstract: Polymerization-induced self-assembly (PISA) is a robust strategy for the syntheses of block copolymer nano-objects with various morphologies. Although PISA has been extensively studied, the use of cyclic macromolecular chain transfer agents (macroCTAs) as the hydrophilic block has not been reported. We explored the effects of macroCTA topology on the polymerization kinetics and morphologies of block copolymer assemblies during reversible addition-fragmentation chain transfer (RAFT) dispersion polymerization. To this end, linear and cyclic poly (ethylene oxide) (PEO) with 4-(4-cyanopentanoic acid) dithiobenzoate (CPADB) groups were synthesized and used as CTAs to mediate the RAFT polymerization of benzyl methacrylate (BzMA) and 2,3,4,5,6-pentafluorostyrene (PFSt) under PISA formulation. Interestingly, the nucleation period of the linear PEO is slightly shorter than that of its cyclic analog, and the cyclic hydrophilic segment leads to a delayed morphological transition during PISA.

Keywords: RAFT polymerization; PISA; cyclic polymer; topological effect

CLC number: O631.3 **Document code:** A

1 Introduction

In recent decades, a variety of macromolecules with complex topologies, including cyclic, star, and hyperbranched polymers, have been synthesized via various synthetic methods. The properties of polymers differ significantly depending on their topology[1–5]. Cyclic polymers have unique properties compared to their linear analogs with the same molar mass due to the lack of chain ends. These properties include lower intrinsic characteristic viscosity, improved heat stability[6–8], and smaller hydrodynamic volume[9,10]. Chemists have extensively investigated the synthetic pathways of cyclic polymers, primarily ring expansion strategies involving the introduction of monomers into cyclic initiators/catalysts or ring-closure techniques via intramolecular coupling of linear precursors terminated with complementary highly reactive groups in dilute solutions[11–15]. Cyclic polymers exhibit unique self-assembly properties[16]. For example, micelles formed by self-assembly of amphiphilic cyclic polymers are smaller in size and more stable than those formed by their linear analogs[17, 18].

Amphiphilic block copolymers (ABCs) often undergo phase separation in selective solvents due to their hydrophilic/hydrophobic nature, forming nanoparticles with diverse morphologies such as micelles, worm-like micelles, lamellae, and vesicles[19–21]. These morphologies are utilized extensively in biomedicine, nanoreactors, catalysis, and other fields[22,23]. The development of controlled radical polymerization (CRP) has provided a versatile strategy for the synthesis of ABCs. This technology significantly facilitates the study of ABCs during self-assembly. Conventional self-assembly of ABCs is usually performed in a dilute solution and involves multiple steps. These tedious and inefficient processes limit the large-scale preparation of nanoparticles, which hinders their potential commercial application[24,25]. Polymerization-induced self-assembly (PISA) is a combination of polymerization and phase separation that facilitates the efficient and scalable preparation of nanoparticles by dispersion or emulsion polymerization in a highly concentrated solution[26–33]. Soluble precursors function as macromolecular chain transfer agents (macroCTAs) and stabilizers in dispersion polymerization systems for PISA, while large amounts of soluble monomers are introduced for CRP. As polymerization proceeds, block copolymers become insoluble at certain critical degrees of polymerization (DP), and spherical micelles develop when microphase separation occurs in the initial polymerization stage. Further growth of the hydrophobic chain segments leads to the emergence of nanoparticles with different morphologies[34–38]. Although PISA has been extensively studied, the majority of currently available nano-objects are composed of linear block copolymers, and cyclic architectures have not been explored to the best of our knowledge. This is a limitation of the PISA approach as topology plays a significant role during phase separation.

Herein, linear poly (ethylene oxide) (PEO) and cyclic PEO (CPEO) with 4-(4-cyanopentanoic acid) dithiobenzoate (CPADB) groups were synthesized and utilized as macroCTAs to prepare nanoparticles by reversible addition-fragmentation chain transfer (RAFT) dispersion polymerization via PISA. Additionally, the influence of topology on the polymerization kinetics and morphology of the block copolymer assemblies was investigated. The nucleation period of the linear PEO (LPEO) was slightly shorter than that of the cyclic analog. The increased solubility of the cyclic hydrophilic segment delayed the morphological transition of the block copolymer nanoparticles during PISA.

2 Materials and methods

2.1 Materials

Benzyl methacrylate (BzMA) and 2,3,4,5,6-pentafluorostyrene (PFSt) were purchased from Aladdin Reagents, China, and stored at −20 °C after removal of the inhibitor with an alkaline alumina column. Styrene (St, 99%) was distilled under reduced pressure and stored at −20 °C. 2,2'-Azobisobutyronitrile (AIBN) was recrystallized from ethanol and stored at 4 °C. Propargyl alcohol was distilled under reduced pressure and stored in the dark until use. Copper(I) bromide (CuBr, 95%) was stirred overnight in acetic acid, filtered, washed thrice with ethanol, and dried under reduced pressure. Sodium azide (NaN_3), 2-bromoisobutyryl bromide (98%), 2,2-dimethylol propionic acid, *N,N′*-dicyclohexylcarbodiimide (DCC), 4-dimethylaminopyridine (DMAP), and triethylamine (TEA, 99%) were purchased from Aladdin Reagent, China and used as received. Poly(ethylene oxide) (PEO-OH, M_n = 4000 g/mol), 9-anthracenecarboxylic acid, *p*-toluene sulfonyl chloride (TsCl), and pentamethyldiethylenetriamine (PMDETA) were purchased from TCI and used as received. Sodium hydroxide (NaOH), anhydrous sodium sulfate (Na_2SO_4), 2,2-dimethoxypropane, concentrated hydrochloric acid (HCl), thionyl chloride ($SOCl_2$), *N,N*-dimethylformamide (DMF), Dichloromethane (DCM) and Tetrahydrofuran (THF) were purchased from Sinopharm Chemical Reagent and were used without further purification. CPADB was synthesized according to a previous study[39].

2.2 Synthesis

2.2.1 Synthesis of PEO-Ts

A 250 mL round-bottom flask was charged with PEO-OH (20.0 g, 5.0 mmol), TEA (28.0 mL, 200.0 mmol), and anhydrous dichloromethane (50.0 mL). The reaction flask was subsequently placed in an iced-water bath. TsCl (1.9 g, 10.0 mmol) dissolved in dichloromethane (2.5 mL) was added dropwise to the reaction mixture and stirred at 50 °C for 12 h after moving placing the flask in an oil bath. The reaction mixture was thrice washed with 1 mol/L HCl (3 × 100.0 mL). The organic phase was subsequently dried with anhydrous Na_2SO_4 and Na_2CO_3. The polymer solution was added dropwise to a large excess of cold diethyl ether (3 × 500.0 mL) to precipitate to obtain PEO-Ts as a white solid (18.8 g, yield 90%).

2.2.2 Synthesis of PEO-N_3

A 250 mL round-bottom flask was successively charged with PEO-Ts (14.0 g, 3.0 mmol), sodium nitride (7.1 g, 60.0 mmol), and DMF (60.0 mL). The mixture was stirred at 90 °C overnight. The DMF was removed by rotary evaporation. The residual NaN_3 was removed by passing through a neutral alumina column. After the removal of DMF and residual NaN_3, the residual polymer was dissolved in THF and subsequently precipitated into a large excess of cold diethyl ether. The polymer was dried under vacuum to yield a white solid (13.6 g, yield 95%).

2.2.3 Synthesis of PEO-ant

AHAnt (Scheme 1) was synthesized as previously reported[40]. A 100 mL reaction flask was successively charged with PEO-N_3 (10.6 g, 2.5 mmol), AHAnt (2.1 g, 5.5 mmol), PMDETA (1.0 mL, 5.0 mmol), cuprous bromide (717.0 mg, 5.0 mmol) and 40.0 mL DMF. The mixture was thoroughly deoxygenated by purging with nitrogen for 30 min. The reaction was allowed to proceed at 60 °C overnight. After the removal of DMF, the residual polymer was dissolved in THF. The copper salt was removed by passing through a neutral alumina column. The THF solution without the copper salt was concentrated and precipitated into cold ethyl ether (3 × 500.0 mL) and dried under vacuum to yield a yellow solid (11.6 g, yield 84%).

2.2.4 Synthesis of CPEO-OH

PEO-ant (100.0 mg, 0.02 mmol) was dissolved in 500 mL anhydrous THF and irradiated with 365 nm UV light for 4 h. When the irradiation was complete, the polymer solution was concentrated, precipitated into cold ether, and dried under vacuum to yield a pale yellow powder (98 mg, yield 98%).

2.2.5 Synthesis of CPEO-CPADB

A 100 mL flask was charged with CPEO-OH (5.0 g, 1.3 mmol), CPADB (2.7 g, 10.0 mmol), DMAP (0.6 g, 5.0 mmol), and anhydrous dichloromethane (50.0 mL). DCC (1.6 g, 7.5 mmol) in 5 mL CH_2Cl_2 was added dropwise to this mixture and stirred at 2 °C for 72 h. The reaction mixture was subsequently filtered and washed with water (3 × 100.0 mL). The organic phase was dried over anhydrous Na_2SO_4, and the solvent was removed under reduced pressure. The concentrated polymer solution was precipitated into cold ethyl ether. A red solid was obtained (5.1 g, yield 95%).

2.2.6 Synthesis of LPEO-CPADB

A 10 mL flask was charged with PEO-OH (5.0 g, 1.3 mmol), CPADB (2.7 g, 10.0 mmol), DMAP (0.6 g, 5.0 mmol), and anhydrous dichloromethane (50.0 mL). DCC (1.6 g, 7.5 mmol) in 5 mL CH_2Cl_2 was added slowly to the reaction mixture and stirred at 2 °C for 72 h. The reaction mixture was subsequently filtered and washed with water (3 × 100.0 mL). The organic phase was dried over anhydrous Na_2SO_4 and the solvent was removed under reduced pressure. The concentrated polymer solution was precipitated into cold ethyl ether. A red solid was obtained (5.2 g, yield 97%).

2.3 Characterization

2.3.1 Nuclear magnetic resonance (NMR)

All NMR spectra were recorded on a Bruker NMR spectrometer (resonance frequency of 400 MHz for ^{1}H) operated in Fourier transform mode. The samples were dissolved in chloroform-d, with tetramethylsilane (TMS) as an internal reference.

DOI: 10.52396/JUSTC-2022-0040
JUSTC, **2022**, 52(5): 1

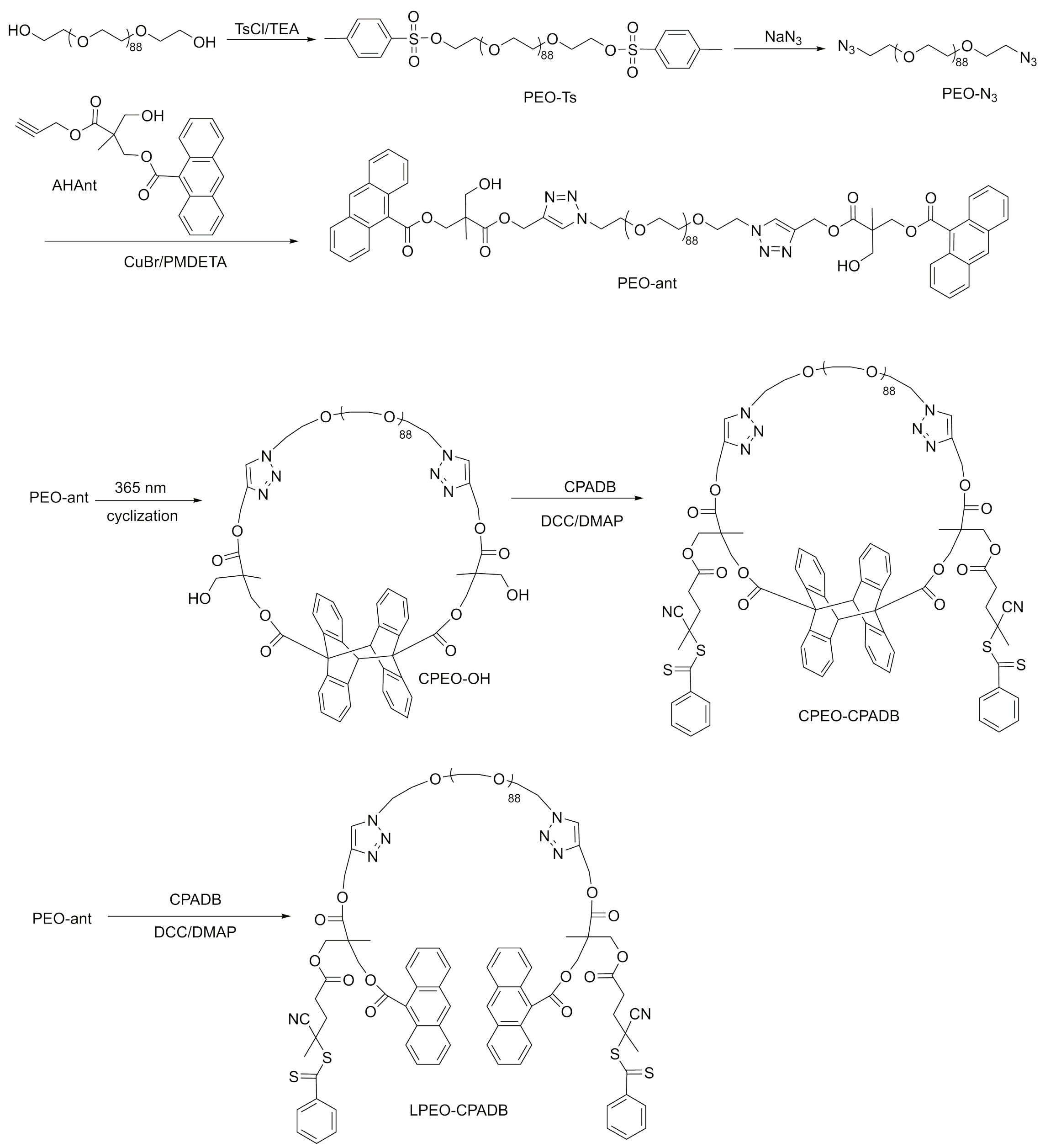

Scheme 1. Synthesis of LPEO-CPADB and CPEO-CPADB.

2.3.2 Gel permeation chromatography (GPC)

Molecular weight and dispersity (*Đ*) were determined using gel permeation chromatography (GPC, Waters 1515) equipped with an RI 2414 detector at 35 °C and microstyragel columns (500, 10^3, and 10^4 Å) calibrated with monodisperse polystyrene standards. THF was used as eluent at a flow rate of 1.0 mL/min.

2.3.3 Transmission electron microscopy (TEM)

TEM was conducted using a Hitachi H-800 electron microscope at an acceleration voltage of 100 kV. To prepare the TEM samples, 10.0 μL of the diluted copolymer solution was placed onto a carbon-coated copper grid and dried in the dark.

2.3.4 Dynamic light scattering (DLS)

DLS was used to determine the size of the nanoparticles on a commercial laser light scattering (LLS) spectrometer (Zetasizer Nano ZS90, Malven Instruments Ltd., Malvern, UK) equipped with a 90° fixed-angle He-Ne laser (4.0 mW, 633 nm). DLS samples were prepared by diluting the nanoparticle dispersion formed by PISA to 0.01% w/w. The tests were performed in triplicate at 25 °C.

3 Results and discussion

3.1 Synthesis of linear and cyclic macroCTAs

The synthetic routes for the two macro-RAFT reagents with different topological structures are shown in Scheme 1. First, anthracene-terminated PEO (PEO-ant) was prepared via sequential esterification, azidation, and click reaction with AHAnt. AHAnt contains multiple functional groups, including an anthryl group for cyclization, a hydroxyl group for es-

DOI: 10.52396/JUSTC-2022-0040
JUSTC, **2022**, 52(5): 1

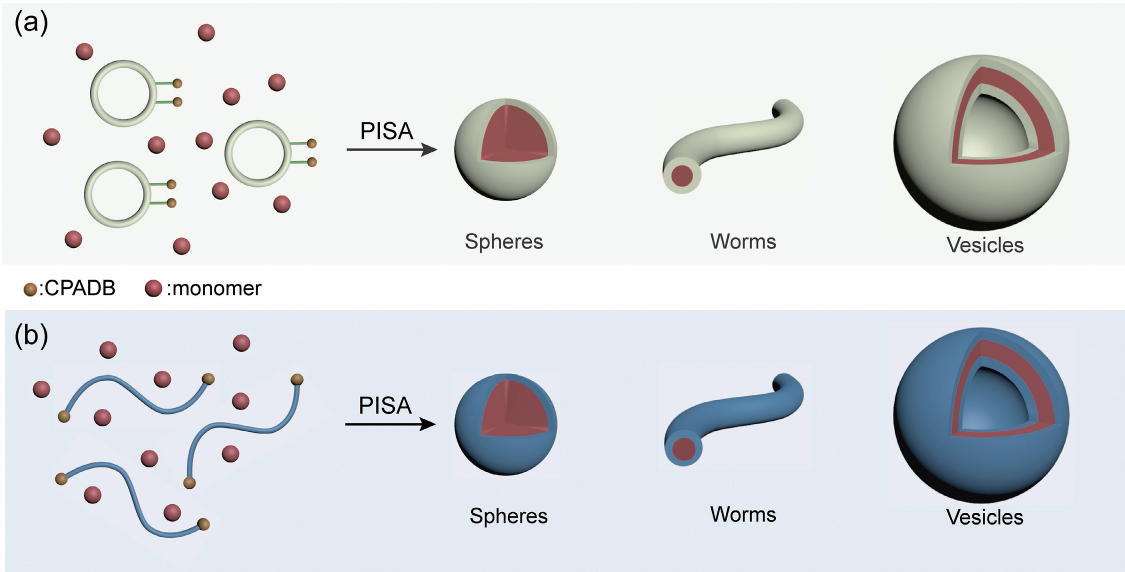

Scheme 2. Synthesis of diblock copolymer nano-objects via polymerization-induced self-assembly (PISA) using (a) CPEO-CPADB and (b) LPEO-CPADB as macroCTA, respectively.

terification, and an alkynyl group for the click reaction. To further obtain the cyclic analog, cyclization was achieved via intramolecular coupling of the anthryl end-groups as previously reported[41]. Linear and cyclic PEO were subsequently modified with CPADB via esterification to afford the macroCTAs. The ^{1}H-NMR spectrum of LPEO-CPADB is shown in Fig. 1a. The peaks at 8.5 ppm (a), 8.0 ppm (b, c), and 7.5 ppm (d, e) are characteristic signals of the aromatic protons of the anthryl groups. The signals at 1.7 ppm (m) and 3.6 ppm (n) are assigned to the methyl protons of CPADB and the ethylene protons of the PEO backbone, respectively. According to the integrated intensity ratio of signals m and n, the grafting efficiency of CPADB onto LPEO-CPADB was calculated as 96%. The GPC trace of LPEO-CPADB, shown in Fig. 2 (black line), is symmetrical and unimodal. The corresponding M_n and M_w/M_n values are 4700 g/mol and 1.05, respectively.

Fig. 1b shows the ^{1}H-NMR spectrum of CPEO-CPADB. Compared with that of LPEO-CPADB, the characteristic signals of the anthryl groups disappeared, and the signals for the anthracene dimer (6.9−6.5 ppm) appeared, indicating that the dimerization reaction proceeded successfully. Similarly, the grafting efficiency of CPADB was calculated as approximately 95%. The GPC trace of CPEO-CPADB, shown in Fig. 2 (red line), is similar to that of LPEO-CPADB with decreased M_n (4700 g/mol for LPEO-CPADB and 4200 g/mol for CPEO-CPADB). This is consistent with decreased hydrodynamic volume owing to its cyclic architecture[42].

3.2 RAFT dispersion polymerization of BzMA mediated by linear and cyclic macroCTAs

In this study, macro-RAFT reagents with linear and cyclic topologies were synthesized. BzMA was selected as the hydrophobic monomer for dispersion polymerization. The effect of topology on polymerization kinetics was investigated by ^{1}H-NMR spectroscopy (Fig. 3). The conversion of BzMA throughout the polymerization reaction was calculated based on the integral ratio of BzMA vinyl protons (6.2−4.8 ppm) and PEO ethylene protons (3.6 ppm). The conversion-time plots, polymerization kinetics, and GPC traces of the block copolymers are shown in Fig. 4. Initially, the rate of BzMA polymerization was low but increased significantly after 3 h (Fig. 4). Additionally, the $\ln([M]_0/[M])$ vs. time plot demonstrates two stages during the polymerization process. Homogeneous polymerization was conducted during the first stage (within 2 h) of polymerization. Initially, the monomer was consumed slowly, and the newly formed copolymer might be dissolved in the solvent. After the formation of spherical micelles (at 2.1 h), heterogeneous polymerization occurred. The apparent enhancement of the polymerization rate after phase separation might be induced by the relatively high local monomer concentration in the nanoparticles and segregated confined reaction environments[43]. The GPC curves of LPEO-*b*-PbzMA shifted to shorter retention times throughout the polymerization. The molecular weight distribution (M_w/M_n) of the synthesized block copolymers is reported in Table 1.

The RAFT dispersion polymerization of BzMA mediated by CPEO-CPADB demonstrated a similar conversion profile to that of LPEO-CPADB (Fig. 4c). The difference lies in the increased homogeneous polymerization phase for CPEO-CPADB (2.5 h), which could be facilitated by the increased solubility of the cyclic macroCTA. GPC traces of CPEO-*b*-PBzMA obtained throughout the polymerization are summarized in Fig. 4d. The detailed M_n and M_w/M_n values are reported in Table 2.

3.3 The preparation of nanoparticles with different morphologies

To assess the effect of macroCTA architecture on the morphological evolution during PISA, a library of PEO-*b*-PBzMA block copolymer nano-objects with increased DP of PBzMA (50, 100, 150, 200, 300, and 400) was synthesized at 20% solid content using linear and cyclic macroCTA (Scheme 2). A polymerization time of 12 h was required to achieve near-quantitative BzMA conversion. The morphologies of the PEO-*b*-PBzMA assemblies were tracked by trans-

DOI: 10.52396/JUSTC-2022-0040
JUSTC, **2022**, 52(5): 1

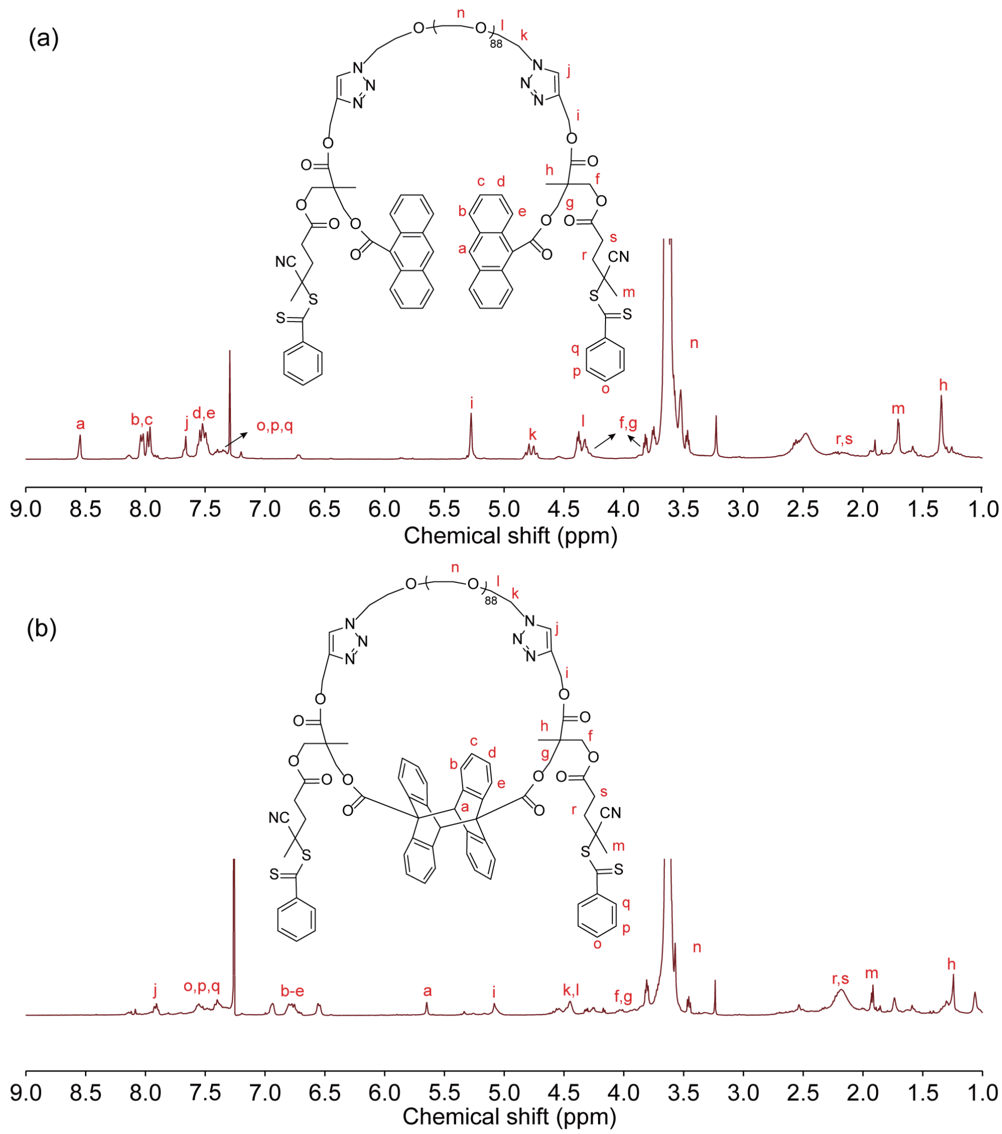

Fig. 1. ^{1}H-NMR spectra of LPEO-CPADB (a) and CPEO-CPADB (b) (in $CDCl_3$).

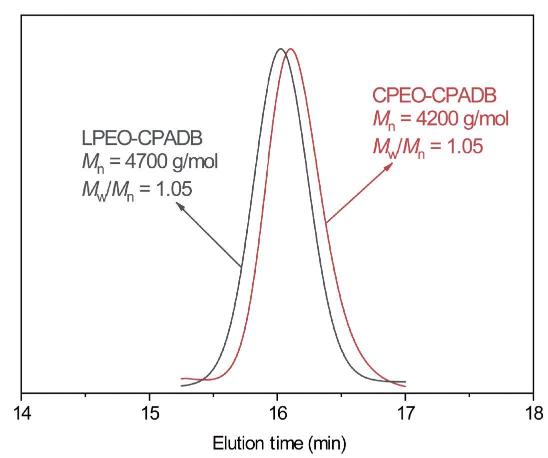

Fig. 2. GPC traces of LPEO-CPADB and CPEO-CPADB with THF as eluent.

mission electron microscopy (TEM) (Fig. 5).

Both LPEO-*b*-PBzMA and CPEO-*b*-PBzMA copolymer nano-objects evolve from spherical micelles to long entangled nanowires, to coexisting of nanowires and lamella, and finally to vesicles, as the PBzMA block increases. However, there are some distinctions between the linear and cyclic morphologies. A morphological transition from spherical to worm-like occurred for linear PEO when BzMA was increased to 150 (LPEG-*b*-$PBzMA_{150}$). However, CPEG-*b*-$PBzMA_{150}$ still demonstrated a spherical morphology. Increasing the DP to afford LPEG-*b*-$PBzMA_{300}$ resulted in a morphological change to vesicles, whereas CPEG-*b*-$PBzMA_{300}$ resulted in worms with a minor population of lamella. The delayed morphological transformation of CPEG-*b*-PBzMA may be attributed to the increased solubility of the cyclic hydrophilic segment[44]. CPEO-*b*-PBzMA copolymers with longer PBzMA segments were more stable than their linear analogs.

To further illustrate the topological effect on the morphology of nanoparticles during PISA, more hydrophobic 2,3,4,5,6-pentafluorostyrene (FSt) was selected as the mono-

DOI: 10.52396/JUSTC-2022-0040
JUSTC, **2022**, 52(5): 1

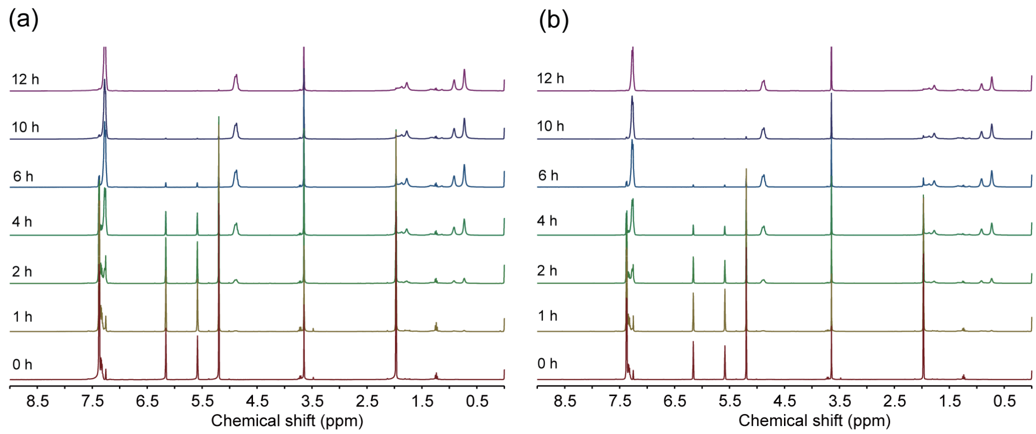

Fig. 3. Polymerizations were conducted using $[BzMA]_0 : [macro\text{-}RAFT\ agent]_0 : [AIBN]_0 = 400:1:0.4$. ^{1}H-NMR spectra of PEO-*b*-PBzMA recorded during the RAFT dispersion polymerization of BzMA using (a) LPEO-CPADB and (b) CPEO-CPADB as the macroCTA in an ethanol/water mixture (70/30, w/w). Solid concentration, 10% w/w (in $CDCl_3$).

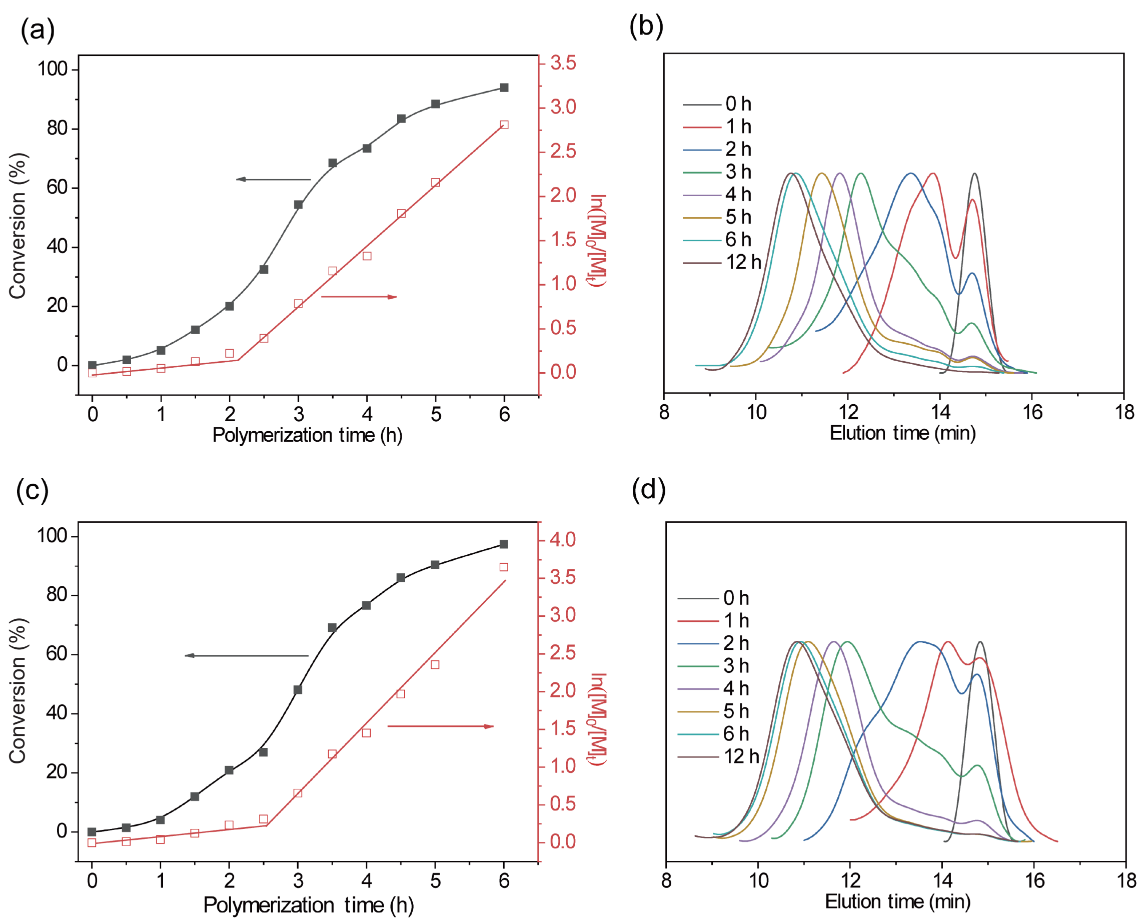

Fig. 4. Conversion vs. time (black line) and $\ln([M]_0/[M]_t)$ vs. time (red line) plots of BzMA during the RAFT dispersion polymerization using (a) LPEO-CPADB and (c) CPEO-CPADB as the macroCTA. GPC traces of (b) LPEO-*b*-PBzMA and (d) CPEO-*b*-PBzMA copolymers were obtained at different polymerization times.

mer. RAFT-mediated dispersion polymerization of FSt was performed in an ethanol/DMF mixture (95/5, w/w) at 70 °C using LPEO-CPADB and CPEO-CPADB as macroCTAs. The target DPs of PFSt were 40, 80, 120, 160, and 200. As shown in Fig. 6, a morphological evolution from spherical micelles (DP = 40) to vesicles (DP > 40) was observed for the LPEO-*b*-PPFSt nano-objects. However, nanowires were observed for CPEO-*b*-PPFSt when the DP of PPFSt was 80 and 120. This result demonstrates the effect of macroCTA architecture on the morphological transitions during PISA.

Table 1. Summary of monomer conversions, actual DP of PBzMA, M_n, and $Đ$ of LPEO-*b*-PBzMA copolymers, and D_{DLS} of LPEO-*b*-PBzMA nano-objects.

Samples	Feed ratio	Time (h)	Conversion (%)	Actual DP	$M_{n,NMR}$ (g/mol)	$M_{n,GPC}$ (g/mol)	M_w/M_n	D_{DLS}(nm)
1	1/0.4/400	0.5	1.9	8	6690	5380	1.12	–
2	1/0.4/400	1.0	5.1	20	8970	6340	1.23	–
3	1/0.4/400	1.5	12.1	48	13890	9900	1.26	125
4	1/0.4/400	2.0	20.0	80	19470	11840	1.23	114
5	1/0.4/400	2.5	32.5	130	28230	21600	1.21	130
6	1/0.4/400	3.0	54.4	218	43680	37570	1.24	237
7	1/0.4/400	3.5	68.6	274	53730	48820	1.23	252
8	1/0.4/400	4.0	73.4	294	57050	51440	1.24	259
9	1/0.4/400	4.5	83.6	334	64200	54850	1.42	267
10	1/0.4/400	5.0	88.5	354	67640	59140	1.24	214
11	1/0.4/400	6.0	94.0	376	71530	63510	1.28	176
12	1/0.4/400	10.0	97.6	390	74080	67070	1.31	218
13	1/0.4/400	12.0	98.6	394	74790	69500	1.35	347

Table 2. Summary of monomer conversions, actual DP of PBzMA, M_n, and $Đ$ of CPEO-*b*-PBzMA copolymers, and D_{DLS} of CPEO-*b*-PBzMA nano-objects.

Samples	Feed ratio	Time (h)	Conversion (%)	Actual DP	$M_{n,NMR}$ (g/mol)	$M_{n,GPC}$ (g/mol)	$Đ$	D_{DLS}(nm)
1	1/0.4/400	0.5	1.5	6	6390	5220	1.10	–
2	1/0.4/400	1.0	4.1	16	8250	6330	1.23	–
3	1/0.4/400	1.5	12.0	48	13780	9720	1.24	114
4	1/0.4/400	2.0	20.9	84	20080	14590	1.27	140
5	1/0.4/400	2.5	27.0	108	24390	17200	1.22	149
6	1/0.4/400	3.0	48.1	192	39230	33080	1.37	154
7	1/0.4/400	3.5	69.1	276	54000	49970	1.25	179
8	1/0.4/400	4.0	76.6	306	59290	51850	1.30	264
9	1/0.4/400	4.5	86.0	344	65930	58000	1.26	220
10	1/0.4/400	5.0	90.5	362	69080	61300	1.23	144
11	1/0.4/400	6.0	91.5	366	69780	62940	1.29	246
12	1/0.4/400	10.0	97.4	390	73930	66500	1.31	278
13	1/0.4/400	12.0	98.0	392	74360	68100	1.34	310

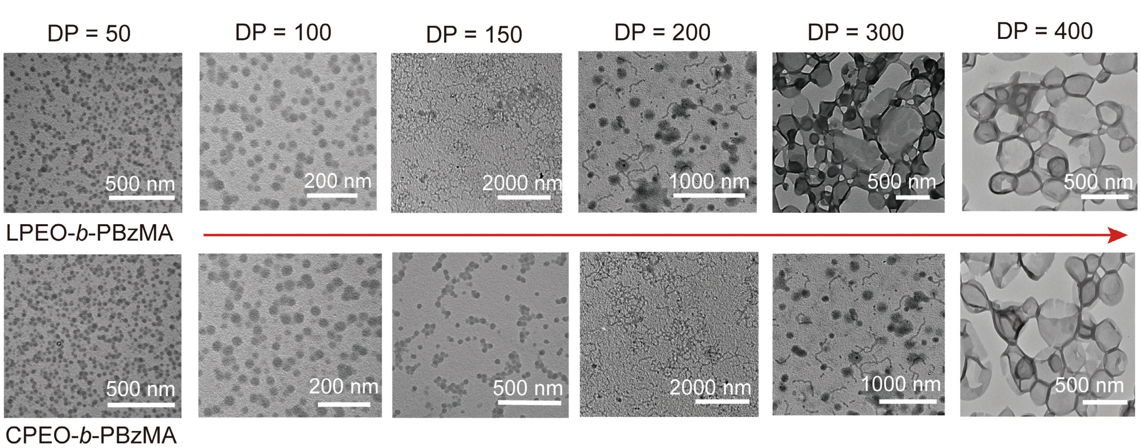

Fig. 5. TEM images of the PEO-*b*-PBzMA copolymer nano-objects with different DPs of PBzMA in the ethanol/water mixture (70/30, w/w), and the solid content = 20% (w/w).

DOI: 10.52396/JUSTC-2022-0040
JUSTC, **2022**, 52(5): 1

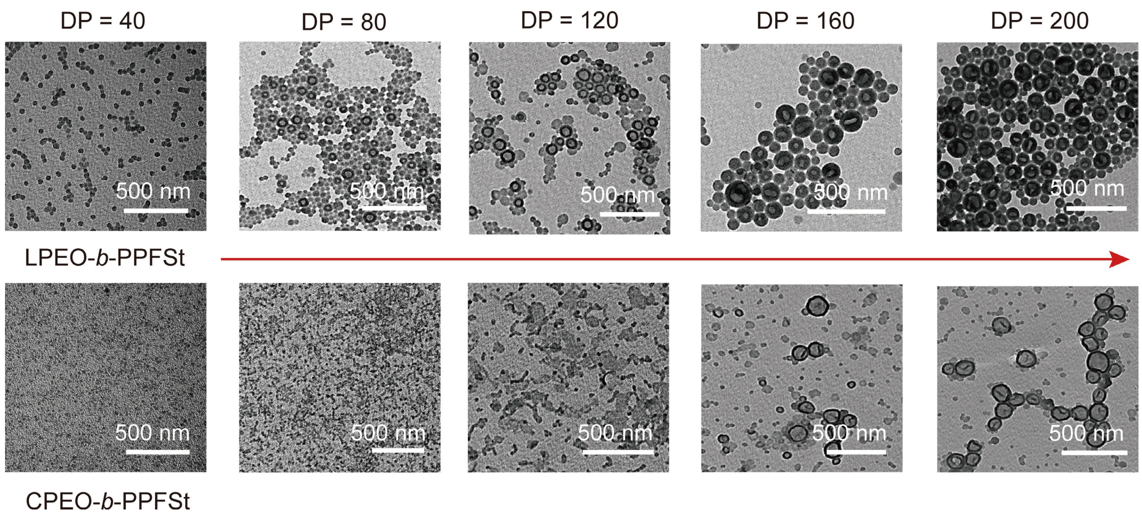

Fig. 6. TEM images of the PEO-*b*-PPFSt copolymer nano-objects with different DPs of PPFSt in the ethanol/DMF mixture (95/5, w/w), and the solid content = 25% (w/w).

4 Conclusions

In summary, RAFT-mediated dispersion polymerization was performed to study the influence of two distinct hydrophilic topologies on the polymerization kinetics and morphological evolution of block copolymer nanoparticles. The polymerization process demonstrated two distinct stages. The nucleation period of the linear analog was slightly shorter than that of the cyclic analog. Different hydrophobic monomers were selected to assess the influence of topology on the morphological evolution of ABC nanoparticles. The increased solubility of the cyclic hydrophilic macroCTA further stabilized the nanoparticles and subsequently delayed morphological transitions during PISA.

Acknowledgements

This work was supported by the National Natural Science Foundation of China (22131010, 52021002) and the Fundamental Research Funds for the Central Universities (WK2060000012).

Conflict of interest

The authors declare that they have no conflict of interest.

Biographies

Depeng Yin is currently a postgraduate student in CAS Key Laboratory of Soft Matter Chemistry, Department of Polymer Science and Engineering under the supervision of Prof. Chunyan Hong at the University of Science and Technology of China. His research mainly focuses on polymerization induced self-assembly.

Chao Liu is currently a postdoctoral fellow at the University of Science and Technology of China (USTC). He received his Ph.D. in Chemistry from USTC in 2019 under the supervision of Profs. Chunyan Hong and Caiyuan Pan. He then joined Prof. Chunyan Hong's group as a postdoctoral fellow in July 2019. His scientific interests include the synthesis of topological polymers and polymerization-induced self-assembly.

Chunyan Hong is a Professor at the University of Science and Technology of China (USTC). She obtained her Ph.D. in Chemistry from USTC in 2002. Her research interests include controlled radical polymerization, the synthesis of stimuli responsive polymers and biodegradable polymers, the fabrication of functionalized nanomaterials, and their applications in drug or gene delivery.

References

[1] Bielawski C W, Benitez D, Grubbs R H. An" endless" route to cyclic polymers. *Science,* **2002**, *297* (5589): 2041–2044.
[2] Gonsales S A, Kubo T, Flint M K, et al. Highly tactic cyclic polynorbornene: Stereoselective ring expansion metathesis polymerization of norbornene catalyzed by a new tethered tungsten-alkylidene catalyst. *J. Am. Chem. Soc.,* **2016**, *138* (15): 4996–4999.
[3] Nadif S S, Kubo T, Gonsales S A, et al. Introducing “ Ynene” metathesis: Ring-expansion metathesis polymerization leads to highly cis and syndiotactic cyclic polymers of norbornene. *J. Am. Chem. Soc.,* **2016**, *138* (20): 6408–6411.
[4] Roland C D, Li H, Abboud K A, et al. Cyclic polymers from alkynes. *Nat. Chem.,* **2016**, *8* (8): 791–796.
[5] Culkin D A, Jeong W, Csihony S, et al. Zwitterionic polymerization of lactide to cyclic poly (lactide) by using N-heterocyclic carbene organocatalysts. *Angew. Chem. Int. Ed.,* **2007**, *119* (15): 2681–2684.
[6] Kapnistos M, Lang M, Vlassopoulos D, et al. Unexpected power-law stress relaxation of entangled ring polymers. *Nat. Mater.,* **2008**, *7* (12): 997–1002.
[7] Di Marzio E A, Guttman C M. The glass temperature of polymer rings. *Macromolecules,* **1987**, *20* (6): 1403–1407.
[8] Clarson S, Semlyen J. Cyclic polysiloxanes: 1. Preparation and characterization of poly (phenylmethylsiloxane). *Polymer,* **1986**, *27* (10): 1633–1636.
[9] Hadziioannou G, Cotts P, Ten Brinke G, et al. Thermodynamic and hydrodynamic properties of dilute solutions of cyclic and linear polystyrenes. *Macromolecules,* **1987**, *20* (3): 493–497.
[10] Jang S S, Çağin T, Goddard III W A. Effect of cyclic chain architecture on properties of dilute solutions of polyethylene from molecular dynamics simulations. *J. Chem. Phys.,* **2003**, *119* (3): 1843–1854.
[11] Tezuka Y, Oike H. Topological polymer chemistry: Systematic classification of nonlinear polymer topologies. *J. Am. Chem. Soc.,* **2001**, *123* (47): 11570–11576.
[12] Tezuka Y, Mori K, Oike H. Efficient synthesis of cyclic poly (oxyethylene) by electrostatic self-assembly and covalent fixation with telechelic precursor having cyclic ammonium salt groups. *Macromolecules,* **2002**, *35* (14): 5707–5711.
[13] Yamamoto T, Tezuka Y. Topological polymer chemistry: A cyclic

DOI: 10.52396/JUSTC-2022-0040
JUSTC, **2022**, 52(5): 1

approach toward novel polymer properties and functions. *Polym. Chem.,* **2011**, *2* (9): 1930–1941.
[14] Kimura A, Hasegawa T, Yamamoto T, et al. ESA-CF synthesis of linear and cyclic polymers having densely appended perylene units and topology effects on their thin-film electron mobility. *Macromolecules,* **2016**, *49* (16): 5831–5840.
[15] Laurent B A, Grayson S M. Synthetic approaches for the preparation of cyclic polymers. *Chem. Soc. Rev.,* **2009**, *38* (8): 2202–2213.
[16] Trachsel L, Romio M, Grob B, et al. Functional nanoassemblies of cyclic polymers show amplified responsiveness and enhanced protein-binding ability. *ACS Nano,* **2020**, *14* (8): 10054–10067.
[17] Honda S, Yamamoto T, Tezuka Y. Topology-directed control on thermal stability: Micelles formed from linear and cyclized amphiphilic block copolymers. *J. Am. Chem. Soc.,* **2010**, *132* (30): 10251–10253.
[18] Honda S, Yamamoto T, Tezuka Y. Tuneable enhancement of the salt and thermal stability of polymeric micelles by cyclized amphiphiles. *Nat. Commun.,* **2013**, *4* (1): 1574.
[19] Discher B M, Won Y Y, Ege D S, et al. Polymersomes: Tough vesicles made from diblock copolymers. *Science,* **1999**, *284* (5417): 1143–1146.
[20] Mai Y, Eisenberg A. Self-assembly of block copolymers. *Chem. Soc. Rev.,* **2012**, *41* (18): 5969–5985.
[21] Discher D E, Eisenberg A. Polymer vesicles. *Science,* **2002**, *297* (5583): 967–973.
[22] Tian H, Qin J, Hou D, et al. General interfacial self-assembly engineering for patterning two-dimensional polymers with cylindrical mesopores on graphene. *Angew. Chem. Int. Ed.,* **2019**, *131* (30): 10279–10284.
[23] Wang Z, Van Oers M C, Rutjes F P, et al. Polymersome colloidosomes for enzyme catalysis in a biphasic system. *Angew. Chem. Int. Ed.,* **2012**, *124* (43): 10904–10908.
[24] Zhang L, Shen H, Eisenberg A. Phase separation behavior and crew-cut micelle formation of polystyrene-b-poly (acrylic acid) copolymers in solutions. *Macromolecules,* **1997**, *30* (4): 1001–1011.
[25] Liu F, Eisenberg A. Preparation and pH triggered inversion of vesicles from poly (acrylic acid)-block-polystyrene-block-Poly (4-vinyl pyridine). *J. Am. Chem. Soc.,* **2003**, *125* (49): 15059–15064.
[26] Foster J C, Varlas S, Couturaud B, et al. Getting into shape: Reflections on a new generation of cylindrical nanostructures' self-assembly using polymer building blocks. *J. Am. Chem. Soc.,* **2019**, *141* (7): 2742–2753.
[27] D'agosto F, Rieger J, Lansalot M. RAFT-mediated polymerization-induced self-assembly. *Angew. Chem. Int. Ed.,* **2020**, *59* (22): 8368–8392.
[28] Cornel E J, Jiang J, Chen S, et al. Principles and characteristics of polymerization-induced self-assembly with various polymerization techniques. *CCS Chem.,* **2021**, *3* (4): 2104–2125.
[29] Zeng M, Zhou S, Sui X, et al. Effect of solvophilic chain length in PISA particles on Pickering emulsion. *Chin. J. Chem.,* **2021**, *39* (12): 3448–3454.
[30] Cai W B, Liu D D, Chen Y, et al. Enzyme-assisted photoinitiated polymerization-induced self-assembly in continuous flow reactors with oxygen tolerance. *Chinese J. Polym. Sci.,* **2021**, *39* (9): 1127–1137.
[31] Charleux B, Delaittre G, Rieger J, et al. Polymerization-induced self-assembly: From soluble macromolecules to block copolymer nano-objects in one step. *Macromolecules,* **2012**, *45* (17): 6753–6765.
[32] Penfold N J, Yeow J, Boyer C, et al. Emerging trends in polymerization-induced self-assembly. *ACS Macro Lett.,* **2019**, *8* (8): 1029–1054.
[33] Jennings J, He G, Howdle S M, et al. Block copolymer synthesis by controlled/living radical polymerisation in heterogeneous systems. *Chem. Soc. Rev.,* **2016**, *45* (18): 5055–5084.
[34] Cai W, Wan W, Hong C, et al. Morphology transitions in RAFT polymerization. *Soft Matter,* **2010**, *6* (21): 5554–5561.
[35] Sun J T, Hong C Y, Pan C Y. Recent advances in RAFT dispersion polymerization for preparation of block copolymer aggregates. *Polym. Chem.,* **2013**, *4* (4): 873–881.
[36] Zhang Y, Han G, Cao M, et al. Influence of solvophilic homopolymers on RAFT polymerization-induced self-assembly. *Macromolecules,* **2018**, *51* (11): 4397–4406.
[37] Huo M, Zeng M, Li D, et al. Tailoring the multicompartment nanostructures of fluoro-containing ABC triblock terpolymer assemblies via polymerization-induced self-assembly. *Macromolecules,* **2017**, *50* (20): 8212–8220.
[38] Li D, Huo M, Liu L, et al. Overcoming kinetic trapping for morphology evolution during polymerization-induced self-assembly. *Macromol. Rapid Commun.,* **2019**, *40* (16): 1900202.
[39] Zhang W J, Hong C Y, Pan C Y. Fabrication of electrospinning fibers from spiropyran-based polymeric nanowires and their photochromic properties. *Macromol. Chem. Phys.,* **2013**, *214* (21): 2445–2453.
[40] Liu C, Fei Y Y, Zhang H L, et al. Effective construction of hyperbranched multicyclic polymer by combination of ATRP, UV-induced cyclization, and self-accelerating click reaction. *Macromolecules,* **2019**, *52* (1): 176–184.
[41] Yamamoto T, Yagyu S, Tezuka Y. Light-and heat-triggered reversible linear–cyclic topological conversion of telechelic polymers with anthryl end groups. *J. Am. Chem. Soc.,* **2016**, *138* (11): 3904–3911.
[42] Tang Q, Wu Y, Sun P, et al. Powerful ring-closure method for preparing varied cyclic polymers. *Macromolecules,* **2014**, *47* (12): 3775–3781.
[43] Warren N J, Mykhaylyk O O, Mahmood D, et al. RAFT aqueous dispersion polymerization yields poly (ethylene glycol)-based diblock copolymer nano-objects with predictable single phase morphologies. *J. Am. Chem. Soc.,* **2014**, *136* (3): 1023–1033.
[44] Gao L, Ji Z, Zhao Y, et al. Synthesis and solution self-assembly properties of cyclic rod–coil diblock copolymers. *ACS Macro Lett.,* **2019**, *8* (12): 1564–1569.

DOI: 10.52396/JUSTC-2022-0040
JUSTC, **2022**, 52(5): 1